

---

# ViF-SD2E: A ROBUST WEAKLY-SUPERVISED METHOD FOR NEURAL DECODING

---

SUBTITLE: FROM ROBUST VISION-FEEDBACK TO BRAIN

Jingyi Feng, Yong Luo, and Shuang Song

Institute of Artificial Intelligence, School of Computer Science, Wuhan University  
{fjy2035, luoyong, songshuang327}@whu.edu.cn

## ABSTRACT

Neural decoding plays a vital role in the interaction between the brain and the outside world. In this paper, we directly decode the movement track of a finger based on the neural signals of a macaque. Supervised regression methods may overfit to actual labels containing noise, and require a high labeling cost, while unsupervised approaches often have unsatisfactory accuracy. Besides, the spatial and temporal information is often ignored or not well exploited by those methods. This motivates us to propose a robust weakly-supervised method, called ViF-SD2E, for neural decoding. In particular, it consists of a space-division (SD) module and a exploration-exploitation (2E) strategy, to effectively exploit both the spatial information of the outside world and the temporal information of neural activity, where the SD2E output is compared with the weak 0/1 vision-feedback (ViF) label for training. Extensive experiments demonstrate the effectiveness of our method, which can be sometimes comparable to supervised counterparts.

**Keywords** Neural decoding, weakly-supervised, space division, vision-feedback

## 1 Introduction

Neural coding and decoding are vital technologies for realizing the brain-computer interface, with diverse potential applications, e.g., facilitating the daily life of paralyzed patients [1]. Existing studies mainly focus on movement, speech, and vision, aiming to gain a scientific understanding of the link between neural activity and the outside world [2]. This paper focuses on locating a macaque’s moving finger by decoding the neural spike signals. Addressing this problem not only has direct positive impacts on the impaired user’s ability to communicate with the world, but also provides a solution for human-computer interaction for healthy users [3]. Furthermore, prostheses, robots, mice, and other devices that fully realize ‘brain control technology’ are becoming reality [4, 5]. For people with a physical disability, a prosthesis can be installed and controlled through neural decoding [6].

The problem of decoding finger movement is described in a pioneer work [7], which finds that there is a correspondence between the direction and location of the movement of the upper limb of a macaque and the spike signal in its motor cortex. Most of the early work on neural decoding are time-independent [8, 9]. However, since the movement is a continuous process, more recent work focuses on exploring time correlations [10, 11]. In recent years, neural network approaches, such as recurrent neural networks and long short-term memory [12, 13], have achieved remarkable performance for neural decoding. However, most of these approaches are often supervised, which may lead to overfitting to noisy target values (e.g., finger positions). Although there are also a few semi-supervised [14], unsupervised [8], and weakly supervised decoding [15] approaches, the spatial and temporal information connecting the external world to neural activity are ignored or not well exploited.

To remedy these drawbacks, we propose a novel weakly-supervised neural decoding method, called ViF-SD2E, which mainly consists of a spatial division (SD) module together with an unsupervised exploration and supervised exploitation (2E) strategy, where only weak 0/1 vision-feedback (ViF) labels are required for training. In particular, the input neural signals are sent to an unsupervised expectation maximization (EM) model to **explore** (induce) some initial prediction results. Since the obtained results are often unreliable, we divide the observable space into several non-overlapping

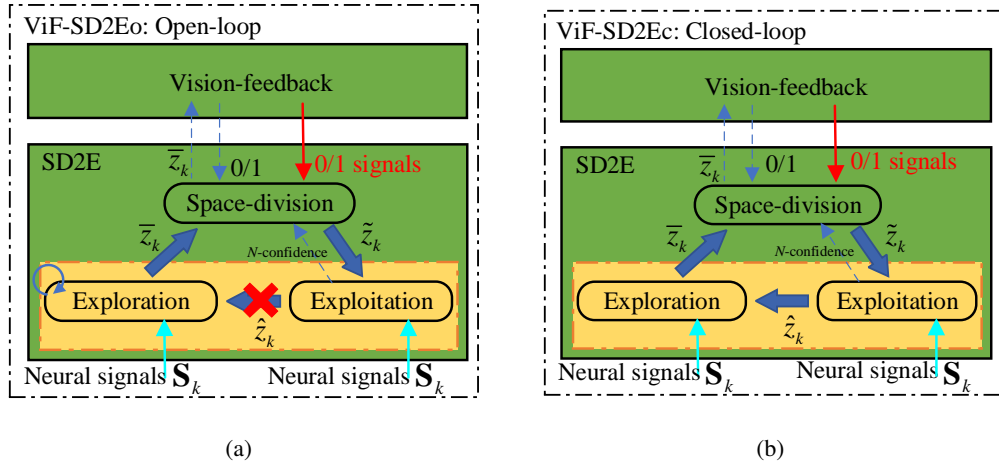


Figure 1: Open-loop (a) and closed-loop (b) optimization procedures of the proposed ViF-SD2E method. Here, the red arrow and the cyan arrow represent the input of vision-feedback from the outside world and the input of neural signals from the brain, respectively. The solid arrow represents the data transmission process and the dashed arrow represents interactive and evaluative feedback, which constitute the training or learning process of the ViF-SD2E.

regions, and assume that there are some weakly-supervised 0/1 labels (vision feedback of the macaque), which indicate the regions in which the target values are located. Here, the space can be divided at different resolutions depending on the degree of supervision. By comparing the binarized initial results and the weak labels, we obtain some corrected outputs. These outputs are then **exploited** in a supervised manner to refine the prediction results, where the temporal information is also exploited. The refined results can be used directly as the final prediction results (open-loop), or to update the parameters of the EM model. The latter leads to a closed-loop optimization, and the exploitation and exploration should iterate until convergence. This often leads to higher prediction performance, but also imposes a higher training cost. Figure 1 is an illustration of the open-loop and closed-loop optimization procedures of the proposed ViF-SD2E method.

The main contributions of this paper are summarized as follows.

- We propose a robust weakly-supervised method for movement decoding via neural signals. Only robust 0/1 signals from the outside world (ViF) are required for model training.
- We design a novel SD module together with a 2E strategy to effectively make use of both the spatial and temporal information for the neural decoding, where the degree of supervision can be flexibly controlled.
- Both open-loop and closed-loop algorithms are developed for optimization.

We conducted extensive experiments on a popular neural decoding dataset. The results demonstrate that our method is superior to other competitive approaches in most cases, and can be comparable or even outperform some supervised counterparts.

## 2 Related work

In our point of view, “visual feedback” can also include any external perception or stimulus in the embodied mind, such as from the eyes, ears, nose, tongue and body. In this paper, we focus on visual object detection, because it is important to locate the target in the motion. In the beginning, many technologies were biased towards supervised methods, then came target detection that applied reinforcement learning [16], and later, unsupervised and self-supervised technology [17]. Recently, interactive target detection technology has been a significant innovation [18]. Last but not least, in our opinion, the working mechanism of the brain’s cognition should include interaction and reinforcement. Here, “reinforcement” refers to the independent thinking of the brain using existing memory or experience (Exploitation), which can also be said to be self-reinforcement.

In addition, state-space models (SSMs) with associations between the current state and the previous state became more developed [19, 1] in neural decoding. Czanner et al. gave an SSM model with generalized linear characteristics that are superior to the traditional model in terms of describing neural activity [20]. Shanechi et al. gave an SSM model

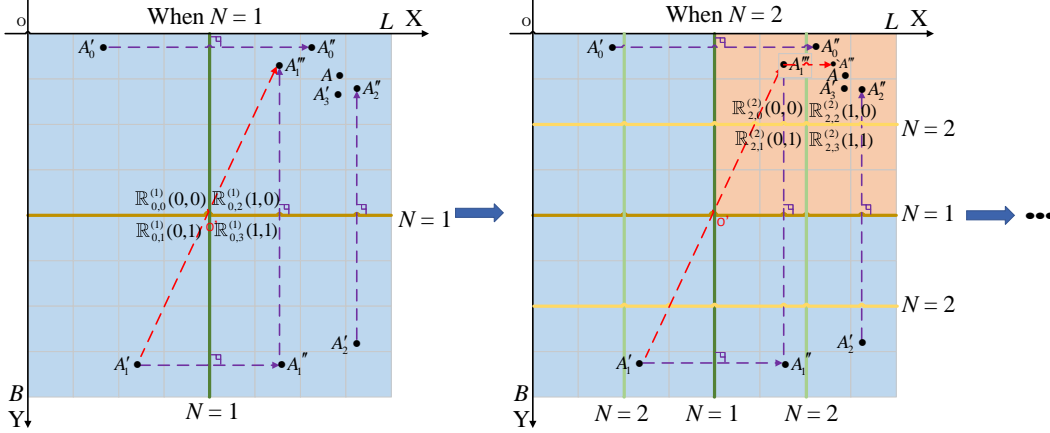


Figure 2: The movement space of the finger that interacts with the brain. Assume that the blue ( $N = 1$ ) and orange ( $N = 2$ ) area are the active space in a certain decoding. The  $A \bullet$  is the real label, and  $A'_0 \bullet$ ,  $A'_1 \bullet$ ,  $A'_2 \bullet$  or  $A'_3 \bullet$  are the unsupervised predicted values that may appear after the exploration. Step 1 ( $N = 1$ ): The 2-D space is divided equally, and their intersection is  $O'$ . Then four subspaces,  $\mathbb{R}_{0,0}^{(1)}(0,0)$ ,  $\mathbb{R}_{0,1}^{(1)}(0,1)$ ,  $\mathbb{R}_{0,2}^{(1)}(1,0)$  and  $\mathbb{R}_{0,3}^{(1)}(1,1)$ , are demarcated. Next, we use spatial symmetry to keep the predicted values and the true labels in one subspace, and obtain  $\bullet A''_0$ ,  $\bullet A''_1$ ,  $\bullet A''_2$  and  $\bullet A''_3$ . Step 2 ( $N = 2$ ): Repeat step 1:  $\mathbb{R}_{0,2}^{(1)}(1,0)$  is divided into four subspaces,  $\mathbb{R}_{2,0}^{(2)}(0,0)$ ,  $\mathbb{R}_{2,1}^{(2)}(0,1)$ ,  $\mathbb{R}_{2,2}^{(2)}(1,0)$ ,  $\mathbb{R}_{2,3}^{(2)}(1,1)$ . Here,  $A \bullet$  is located in  $\mathbb{R}_{2,2}^{(2)}(1,0)$ . Then we also employ spatial symmetry to keep them in one subspace, and get  $\bullet A''_0$ ,  $\bullet A''_1$ ,  $\bullet A''_2$  and  $\bullet A''_3$ . As  $N \rightarrow +\infty$ , our predicted values will gradually approach the true labels in the ViF/SD module.

and used optimal feedback control to decode the movement state [21]. Based on that SSM model, Wu et al. derived a convolutional space model (CSM), which correlates the current state with the neural signals at multiple previous moments [11]. In recent years, deep learning has been the object of a large number of studies in neural decoding, such as RNN [22] and LSTM [23, 24]. The decoding performed by these methods is more accurate than that of the independent linear method.

Furthermore, Wu et al. proposed an unsupervised cubature Kalman filter (UCKF) by exploring the relations between the neural signals and the movement [8]. Due to the instability of this unsupervised model, Feng et al. found that the part/all of the unsupervised decoding positions was reversed in the movement region, leading to significant errors. Then, they introduced a priori binary to verify the existence of this reverse mechanism [25, 15]. Finally, Sussillo et al. found that the source of the recorded neural activity can change from day to day, e.g., due to a slight movement of the implanted electrodes. The proposed multiplicative RNN allows mappings from the neural input to the motor output to partially change from neural activity [26]. Therefore, ViF-SD2E is also robust, which partially allows mapping to change the recorded movement from the outside world, so it can have strong robustness and fault tolerance.

### 3 The space-division and exploration–exploitation with vision-feedback (ViF-SD2E)

The proposed ViF-SD2E is mainly derived from an experimental finding: that is, the unsupervised predicted values in the exploration and the actual labels have partial or full symmetry in the 2-D space [15]. The function of the vision-feedback (ViF) is to provide effective 0/1 feedback to the SD2E; the function of the SD module is to process the information from the exploration and to be a tool for a state transition area from the external world to the SD2E; the function of the exploration from the 2E strategy is to be a tool for unsupervised exploration; the function of the exploitation from the 2E strategy is to be a tool for supervised training. Finally, trained exploitation is used for testing and further used to evaluate the  $N$ -confidence of the corrected position output by the SDE (SD Exploration).

#### 3.1 The vision-feedback (ViF) from the outside world and coding mechanism

First, the movement space has length  $L$  and width  $B$ , such as the size of the screen or that of the field of view. The origin is the upper left corner. Like vision-feedback from humans, we can know which subspace the finger has moved, but its location cannot be readily given by us in a robust fashion. In this paper, the actual labels are encoded as 0/1 signals in

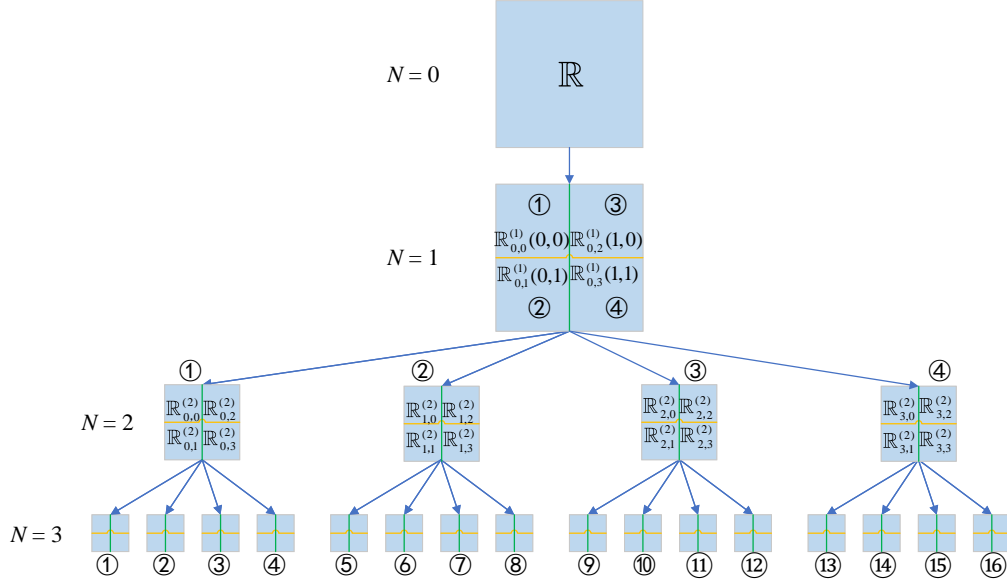


Figure 3: Intuitive diagram of space division in the movement space.

the movement space/subspace and used to extract the maximum and minimum values of the active space/subspace, which are used as the external information (ViF) received during the training of the SD2E. So the total number of subspaces is  $S(N) = 2^{2N}$ . In addition, the maximum fault tolerance of the ViF-SD2E is  $R(N) = L/2^N$  along the  $x$ -axis and  $R(N) = B/2^N$  along the  $y$ -axis (see subsection 4.4). Here,  $N$  is a spatial parameter to control the change from space to subspace. This is shown in Figures 2 and 3.

We will now explain the coding mechanism using an example. The movement space is represented as  $\mathbb{R}$ . The meaning of its subspace  $\mathbb{R}_{n,i}^{(N)}(x_{bit}, y_{bit})$  is the  $i$ th quadrant of the  $n$ th subspace of the  $N$ th divided space, where  $N$  indicates the  $N$ th division of the space,  $n$  is the  $n$ th subspace,  $i$  is the  $i$ th quadrant, and  $x_{bit}$  and  $y_{bit}$  are the encoded  $x$ -position and  $y$ -position in the  $xy$ -plane, as shown in Figure 3. When  $N = 0$ , it is itself, that is,  $\mathbb{R}: \mathbb{R}^{(0)}(0/1, 0/1)$ . When  $N = 1$ ,  $\mathbb{R}$  has been equally divided into four subspaces, namely,  $\mathbb{R}^{(1)}: \mathbb{R}_{0,0}^{(1)}(0, 0), \mathbb{R}_{0,1}^{(1)}(0, 1), \mathbb{R}_{1,0}^{(1)}(1, 0), \mathbb{R}_{1,1}^{(1)}(1, 1)$ . When  $N = 2$ , each subspace of  $\mathbb{R}^{(1)}$  has been equally divided into four subspaces, and there are now 16 subspaces in all. When  $N = 3$ ,  $\mathbb{R}^{(2)}$  has been divided into 32 subspaces in all, and so on. That is, if an actual  $z_k(x_k, y_k)$  is encoded as  $z_k: \mathbb{R}^{(0)}(0/1, 0/1) \rightarrow \mathbb{R}_{0,1}^{(1)}(0, 1) \rightarrow \mathbb{R}_{1,3}^{(2)}(1, 1) \rightarrow \mathbb{R}_{4,1}^{(3)}(0, 1) \rightarrow \dots$ , then the  $x$ - and  $y$ -axes in the actual coordinate  $z_k$  are encoded as  $x_k: 0/1 (\mathbb{R}^{(0)}) \rightarrow 0 (\mathbb{R}^{(1)}) \rightarrow 1 (\mathbb{R}^{(2)}) \rightarrow 0 (\mathbb{R}^{(3)}) \dots; y_k: 0/1 (\mathbb{R}^{(0)}) \rightarrow 1 (\mathbb{R}^{(1)}) \rightarrow 1 (\mathbb{R}^{(2)}) \rightarrow 1 (\mathbb{R}^{(3)}) \dots$

Next, as shown above, the coding mechanism and symmetric correction are used to keep the predicted values and the true labels in the same subspace. Therefore, the calculation of the movement encoder and corrector is given as follows:

$$\lim_{\mathbb{R}: N \rightarrow +\infty} F_{bit}^{(N)} = \begin{cases} 1 & \text{if } \bar{z}_k \text{ or } z_k \geq f_{mid} \\ 0 & \text{if } \bar{z}_k \text{ or } z_k < f_{mid} \end{cases} \quad (1)$$

$$\lim_{\mathbb{R}: N \rightarrow +\infty} F_{update}^{(N)} = \begin{cases} \bar{z}_k & \text{if } \bar{z}_{k,bit} = z_{k,bit} \\ 2(f_{mid} - \bar{z}_k) + \bar{z}_k & \text{if } \bar{z}_{k,bit} \neq z_{k,bit} \end{cases} \quad (2)$$

here,  $\lim_{\mathbb{R}: N \rightarrow +\infty} F_{bit}^{(N)}$  indicates that as the  $N$ -value is increased in  $\mathbb{R}$ , the position that is encoded approaches the subspace where the true label is located.  $F_{bit}^{(N)}$  are the encoded 0/1 signals, such as  $\bar{z}_{k,bit}$  or  $z_{k,bit}$  during the  $N$ th division.  $f_{mid} = (z_{max} + z_{min})/2$  is the central axis of the space/subspace, and  $z_{max}$  and  $z_{min}$  are the maximum and minimum boundaries of the movement during the  $N$ th division. In the corrector,  $\lim_{\mathbb{R}: N \rightarrow +\infty} F_{update}^{(N)}$  indicates that as the  $N$ -value is increased in  $\mathbb{R}$ , the position that is corrected approaches the true label.  $F_{update}^{(N)}$  is the corrected/updated value in the  $N$ th division. Beside, we define the function  $Z(\bullet)$ , which represents the synergy of  $F_{bit}^{(N)}$  and  $F_{update}^{(N)}$ .  $k$  refers to the  $k$ -th moment or the  $k$ -th sample.

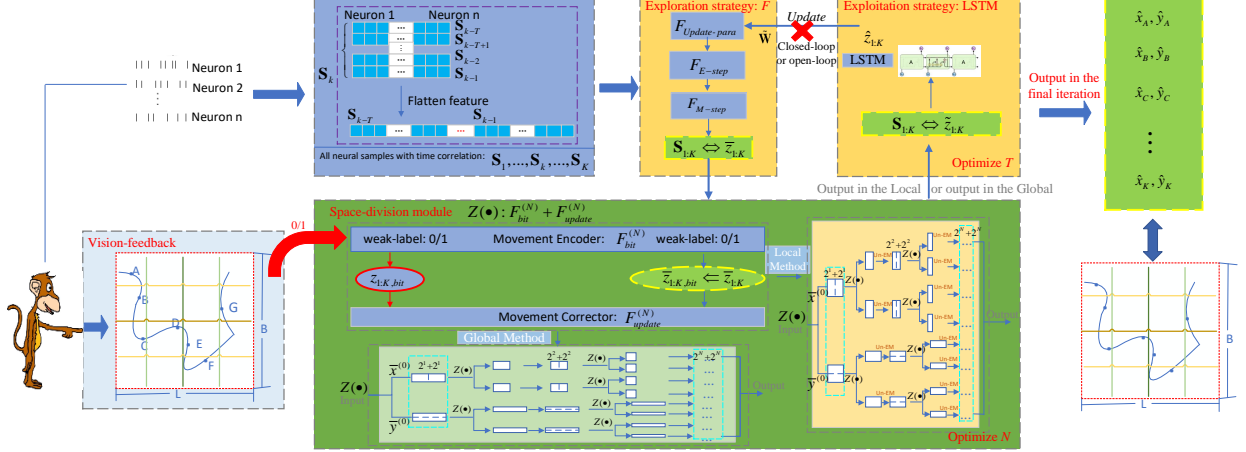


Figure 4: The framework of the proposed ViF-SD2E. In the training phase: 1) the neural signals that have a one-to-one correspondence with the movement of the finger are collected, and the movements are encoded as 0/1 signals via the ViF; the neural signals corresponding to each sample are preprocessed as feature  $\mathbf{S}_k$  together with a time sequence, which is the input to our ViF-SD2E. 2) Then, the  $\bar{z}_{1:K}$  predicted by the exploration are fed into the designed ViF/SD module, where they are encoded as  $\bar{z}_{1:K,bit}$  and compared with the given  $z_{1:K,bit}$ . After being processed by global or local methods, the  $\bar{z}_{1:K}$  is corrected to  $\hat{z}_{1:K}$ ; in the exploitation; the  $\hat{z}_{1:K}$  are then used as ground truth to train the exploitation together with the input feature  $\mathbf{S}_{1:K}$ . Next, if ViF-SD2Ec is being used in its closed-loop mode, the  $\hat{z}_{1:K}$  output by the exploitation is used to update the weight  $\tilde{\mathbf{W}}$  of the exploration. But if ViF-SD2Ec is being used in its open-loop mode, the exploitation's outputs are not used, and the exploration is independent, to form a self-iteration until convergence. Finally, the trained exploitation is adopted for testing and further used to evaluate the  $N$ -confidence.

As  $N \rightarrow +\infty$ , ViF-SD2E can be equivalent to a supervised model, and when  $N = 0$ , it is an unsupervised mode. When  $N$  is set between these two, this can be understood as a weakly-supervised mode. It is worth noting that only the encoded 0/1 signals participate in the feedback, as if we are telling SD2E whether its unsupervised predicted values are good or not. That is, formula (1) is used as an auxiliary of formula (2); the core of formula (2) is that there is a symmetry between  $\bar{z}_k$  and the  $z_k$  in the movement space/subspace.

### 3.2 Spatio-temporal mining in ViF-SD2E

Here, we use the term ‘interaction learning’ to refer to a learning method realized by interaction/feedback between the brain and the external world. In line with our point of view, we refer to the ability to achieve both interaction and self-reinforcement as ‘the brain’s reinforcement’ or ‘the cognitive reinforcement.’ That is, we refer to the ViF-SD2E’s learning as ‘interactive learning with weak-supervision.’ ViF-SD2E includes local and global methods in its open-loop and closed-loop modes. Figure 4 presents the framework of the ViF-SD2E.

#### 3.2.1 The exploration from 2E strategy

The purpose of the exploration is to mine as much as possible the hidden paradigm in neural signals. The unsupervised exploration has an iterative process to convergence. When the exploration’s parameters are updated via the exploitation’s output, ViF-SD2E is in closed-loop; when the exploration’s parameters are updated via self-iteration, ViF-SD2E is in open-loop. In this paper, an EM algorithm is used, which is based on the SSM principle. In the iterative process, the E-step and M-step are defined [27]. The weight is updated as [15]:

$$\tilde{\mathbf{W}} = \left[ \frac{K \sum_{k=1}^K \mathbf{S}_k \hat{z}_k - \sum_{k=1}^K \hat{z}_k \sum_{k=1}^K \mathbf{S}_k}{\sum_{k=1}^K (\hat{z}_k^2 + P_k) - \sum_{k=1}^K \hat{z}_k}, \frac{1}{K} \left( \sum_{k=1}^K \mathbf{S}_k - \bar{\mathbf{a}} \sum_{k=1}^K \hat{z}_k \right) \right]^T \quad (3)$$

where  $\tilde{\mathbf{W}}$  is the updated weight.  $\bar{\mathbf{a}}$  is equivalent to  $\mathbf{a}$  in  $\tilde{\mathbf{W}} = [\mathbf{a}, \bullet]$ .  $\hat{z}_k$  is the position output by the exploitation in each iteration of ViF-SD2E (closed-loop) or the predicted position in each iteration of the EM (open-loop).  $\mathbf{S}_k$  are the input neural signals.  $K$  is the data length.  $P_k$  is the covariance of  $\hat{z}_k$  at time  $k$ .

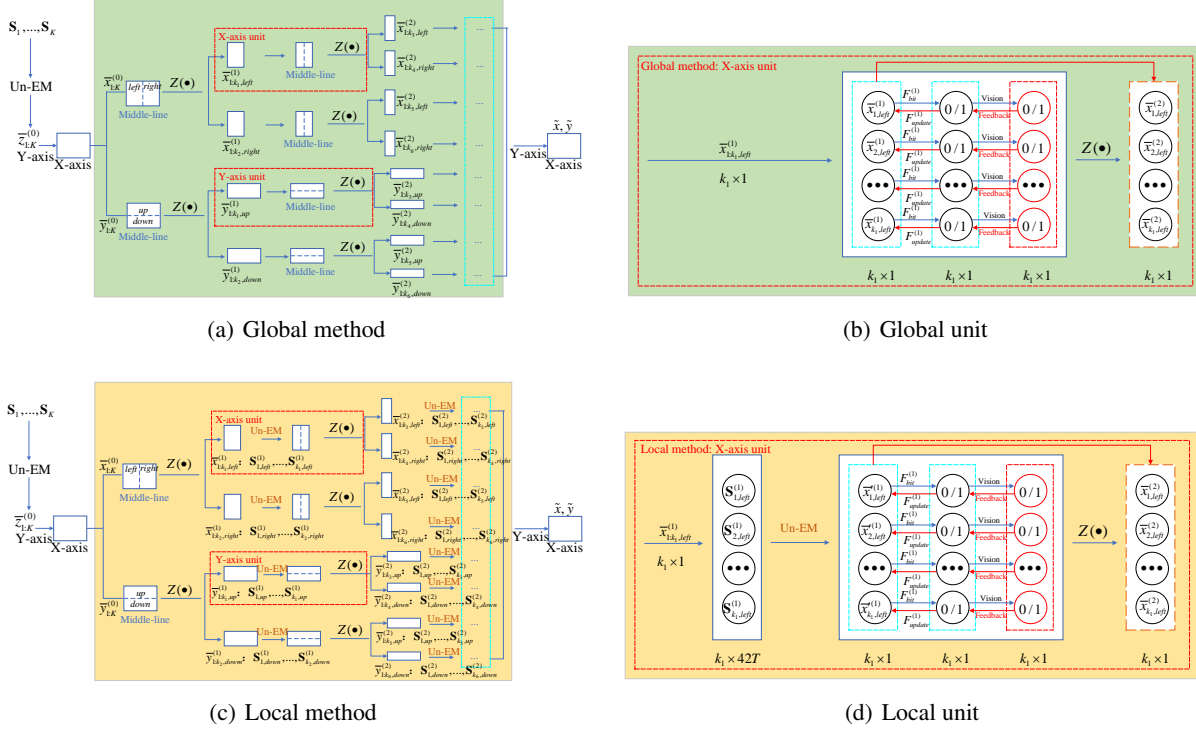


Figure 5: The red box represents the smallest processing unit in the global and local methods. (a) The steps of the global method. What the global method is concerned about is that the unsupervised predicted  $\bar{x}_{1:K}^{(0)}$  and  $\bar{y}_{1:K}^{(0)}$  are sent directly to the equation (1)-(2) for coding and correction. Furthermore, the output of the global method is the corrected  $\tilde{x}_{1:K}^N$  and  $\tilde{y}_{1:K}^N$ . (b) The processing unit of the global method.  $\bar{x}_{1:k_1, left}^{(1)}$  indicates that in the first division, the samples of the  $x$ -axis in the left subspace are taken, and the total number of samples is  $k_1$ . Next,  $\bar{x}_{1:k_1, left}^{(1)}$  is coded as 0/1 by  $F_{bit}^{(1)}$  and compared with the given 0/1, and then corrected by  $F_{update}^{(1)}$ . Finally, the output is  $\bar{x}_{1:k_1, left}^{(2)}$ . (c) The steps of the local method. (d) The processing unit of the local method. The biggest difference between local and global is that in the local unit, the neural signal  $S_{1:k_1, left}^{(1)}$  corresponding to  $\bar{x}_{1:k_1, left}^{(1)}$  is processed by an unsupervised algorithm (Un-EM) to obtain  $\bar{x}_{1:k_1, left}^{(1)}$ , instead of the source  $\bar{x}_{1:k_1, left}^{(1)}$ .

### 3.2.2 The global method and local method from robust SD module

Figure 5 shows the processing steps of the global and local methods. The functions of the global and local methods are obtained by the infinite expansion of the global unit and local unit, respectively. It can be seen from the figure that after each processing unit, the space where the predicted/corrected values are located is divided into two parts, left and right in the  $x$ -axis or up and down in the  $y$ -axis. When  $N = 0$ , ViF-SD2E is an unsupervised model without interaction. As  $N$  increases, the corrected values will gradually approach the subspace where the actual labels are located on the  $x$ -axis or the  $y$ -axis. In the global method, neural signals are not reused for movement prediction in the SD module. In the local method, neural signals complete their self-organization via 0/1 signals for movement prediction of the next subspace. Our goal is to keep the corrected values and the actual labels in one subspace from  $N = 1$  to  $N = +\infty$ . So, the main difference between the local method and the global method is whether the neural signals are reused or not in each subspace. Finally, the output corrections in each subspace are restored to the original space.

### 3.2.3 The exploitation from 2E strategy

The purpose of the exploitation is to memorize or store the output of SDE (space-division exploration); that is, the exploration uses the corrected values and the original input neural signals to train an algorithm. In the training, the output of the exploitation is used to update weight  $\tilde{W}$  of the exploration (closed-loop) or else not used (open-loop). In the testing, the trained exploitation is used for testing and can also prove the validity or  $N$ -confidence of the SDE's output. Here, we choose a classic LSTM as the network skeleton to prove the effectiveness of our work.

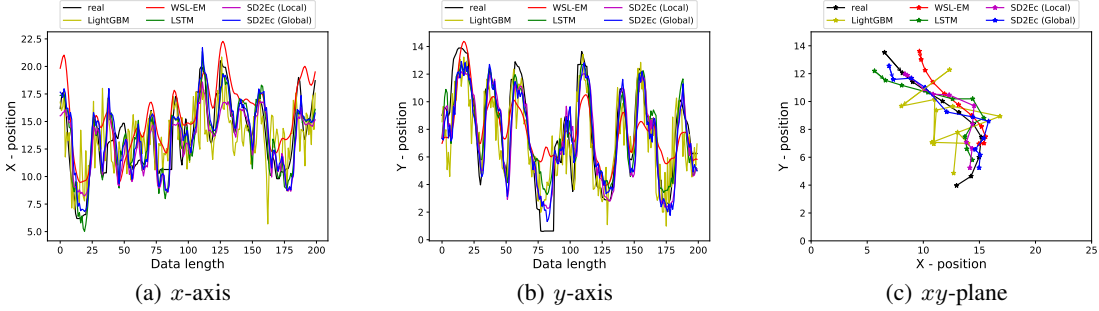


Figure 6: The movement trajectory decoded via neural signals in Experiment A.

Table 1: The comparison experiment for ViF-SD2E and other algorithms in Experiments A and B

Algorithm	Experiment ( $x, y$ )A	RMSE ( $xy$ )A	Experiment ( $x, y$ )B	RMSE ( $xy$ )B	RMSE ( $xy$ ) (A+B)/2
KF [1]	(4.569, 2.974)	5.452	(3.602, <b>1.649</b> )	3.962	4.707
XGBoost [28]	(3.789, 2.590)	4.590	(3.753, 2.103)	4.302	4.446
LightGBM [29]	(3.841, 2.464)	4.563	(3.735, 2.073)	4.272	4.178
WSL-KF [15]	(5.403, 3.202)	6.281	(3.703, 1.754)	4.097	5.189
WSL-EM [15]	(4.518, 2.707)	5.267	(3.398, 2.074)	3.981	4.624
LSTM [24]	(3.384, 2.330)	4.109	<b>(3.337, 1.829)</b>	<b>3.805</b>	3.957
ViF-SD2Ec (Local)	(3.341, 2.296)	4.054	(3.448, 1.916)	3.945	4.000
ViF-SD2Ec (Global)	(3.362, <b>2.191</b> )	<b>4.013</b>	(3.386, 1.900)	3.883	<b>3.948</b>
ViF-SD2Eo (Local)	<b>(3.312, 2.302)</b>	4.033	(3.436, 1.915)	3.934	3.984
ViF-SD2Eo (Global)	(3.394, 2.215)	4.053	(3.504, 1.902)	3.987	4.020

Finally, we believe that the main point of the proposed ViF-SD2E should be the robustness and fault tolerance shown by the ViF/SDE (ViF/SD Exploration) so that the trained exploitation can reach the level of accuracy of a supervised one. Also, the robust sequence 0/1 signals from the external world (ViF) enter the SD2E to make the neural signals of the brain have the ability to self-organize themselves for movement prediction (the local method).

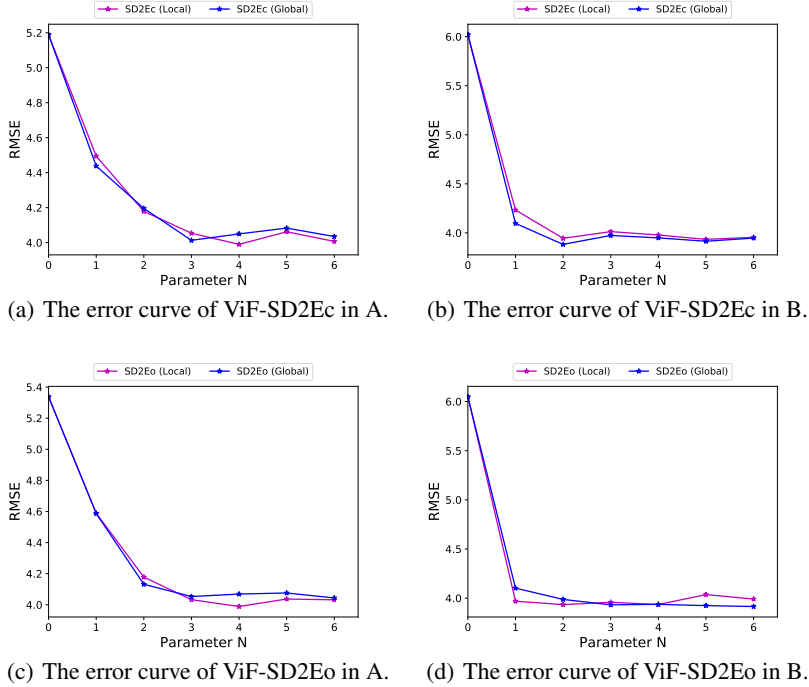
## 4 Experiments

### 4.1 Data set collection

The data was collected and can be found at <https://booksite.elsevier.com/9780123838360/> -> Chapter Materials -> Chapter 22 -> Chap22\_ContinuousTrain (data 1) and Chap22\_ContinuousTest (data 2) [1]. The sampling period is 70 ms. This is about 14.286 Hz, and the total sampling time of 3103 samples is about 217.21 seconds. The specific characteristics are as follows: **Data 1:** The feature matrix is size  $K_1 \times 42$  in data 1; it has  $K_1$  rows and 42 columns, where  $K_1 = 3103$  is the number of samples, and the feature dimension (number of neural signals) of each sample is 42. The position matrix is of size  $K_1 \times 2$ , it has  $K_1$  rows and 2 columns, where the first column is the  $x$ -axis, and the second column is the  $y$ -axis. **Data 2:** The format of data 2 is similar to that of data 1. The feature matrix is size  $K_2 \times 42$ .  $K_2 = 3103$  is the number of samples, and each sample's feature dimension (number of neural signals) is 42. The position matrix is of size  $K_2 \times 2$ . The first column is the  $x$ -axis, and the second column is the  $y$ -axis. For other introductory observations, refer to [15]. Each sample has two labels containing the  $x$ - and  $y$ -position. Because the labels of the  $x$ - and  $y$ -axis are independently predicted, we do the following: **Experiment A:** Data 1 (3103  $x$ -axis samples + 3103  $y$ -axis samples) is used as the training set, and Data 2 (3103  $x$ -axis samples + 3103  $y$ -axis samples) is used as the testing set. **Experiment B:** Data 2 is used as the training set, and Data 1 is used as the testing set. The evaluation measure is the root mean square error.

### 4.2 Decoding results and analysis

Figure 6 shows the movement of the  $x$ - and  $y$ -axes for the 200 samples selected in Experiment A. Firstly, in Figure 6(a), the decoded movement of the ViF-SD2Ec almost well follow the real trajectory, like that of supervised LSTM on the

Figure 7: The error curve of the ViF-SD2Ec and ViF-SD2Eo with parameter  $N$  in Experiments A and B.

$x$ -axis. Next, we will focus on the weakly-supervised methods. Although WSL-EM tracks the movement, it does not do this as well as the other algorithms, such as the 10-30, 60-80, and so on. Secondly, in Figure 6(b), the movement on the  $y$ -axis is given. The performance of each algorithm on the  $y$ -axis is almost the same as that of each algorithm on the  $x$ -axis. Finally, in Figure 6(c), 11 samples are selected from Figure 6(a) and 6(b) for visualization in the  $xy$ -plane. Overall, the decoded movement in the ViF-SD2Ec seems to be a little closer to the real trajectory.

Table 1 lists the errors of the ViF-SD2E (ViF-SD2Ec and ViF-SD2Eo) compared with other algorithms in A and B. Firstly, the minimum error of the ViF-SD2Ec (Global) is 3.948 in the mean error of (A+B) and is about 0.2% lower than that of the supervised LSTM, which implies that the trained exploitation (LSTM) has also reached a supervised level, and further indicates that the correction output by the ViF/SDE (ViF/SD Exploration) has higher  $N$ -confidence. Then, ViF-SD2E in Experiment A shows better performance. However, ViF-SD2E in Experiment B does not improve the performance well. A possible reason for this is that the training samples in Experiment B are more diverse for supervised mode, or perhaps ViF-SD2E’s parameters have not been adjusted to the optimal level (see subsection 4.3). Finally, there are no large differences between ViF-SD2Eo and ViF-SD2Ec in decoding the movement with the local and global methods, but the calculational burden of ViF-SD2Eo is higher than that of ViF-SD2Ec (see subsection 4.5).

### 4.3 Spatial parameter and ablation experiment in ViF-SD2E

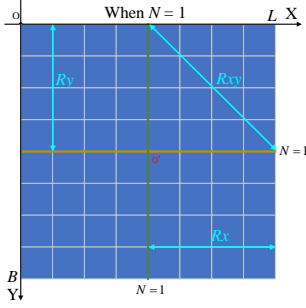
Figure 7 shows the error curves of ViF-SD2E (ViF-SD2Ec and ViF-SD2Eo) in Experiments A and B when  $N$  increases. As shown in Figure 7 (a) to (d), when  $N = 1$ , the decoding errors have dropped sharply because the unsupervised mode with  $N = 0$  has changed to the weakly-supervised mode with  $N = 1$ . After  $N = 3$  or  $N = 4$ , the error basically fluctuates at a low level until convergence. From the above, since the decoding errors may decline if we continue to increase  $N$ , the ViF-SD2E may outperform or be close to the supervised LSTM. In addition, the initial decline of ViF-SD2Eo seems to be faster than that of ViF-SD2Ec from  $N = 0$  to  $N = 3$ . Finally, it should be noted that  $N = 3$  is an appropriate convergence and is what has been set throughout this paper. That is,  $N = 3$  has higher confidence.

Table 2: Ablation for ViF-SD2Ec in Experiment A

Algorithm	RMSE ( $x, y$ )	RMSE ( $xy$ )
Un-EM	(6.870, 3.610)	7.761
Un-EM & LSTM	(4.403, 2.949)	5.298
Un-EM & SD (Local)	(4.066, 2.907)	4.998
Un-EM & SD (Global)	(4.208, 2.771)	5.038
ViF-SD2Ec (Local)	<b>(3.341, 2.296)</b>	4.054
ViF-SD2Ec (Global)	<b>(3.362, 2.191)</b>	<b>4.013</b>

Table 3: The correction experiment for training and testing in Experiments A and B

Algorithm	Uncorr/corr	RMSE	Uncorr/corr	RMSE	RMSE( $xy$ )
	train( $xy$ ) A	Test( $xy$ ) A	train( $xy$ ) B	Test( $xy$ ) B	(A+B)/2 Uncorr/corr/Test
ViF-SD2Ec (L)	6.585/1.491	4.054	10.236/1.171	3.945	8.411/1.331/4.000
ViF-SD2Ec (G)	6.585/1.463	4.013	10.236/1.455	3.883	8.411/1.459/3.948
ViF-SD2Eo (L)	7.141/1.491	4.033	10.366/1.171	3.934	8.754/1.331/3.984
ViF-SD2Eo (G)	7.141/1.506	4.053	10.366/1.378	3.987	8.754/1.442/4.020

Figure 8: The fault tolerance  $R$  in ViF-SD2E.Table 4: Robustness in ViF-SD2E ( $L \approx 25$ ,  $B \approx 15$ )

Parameter	$R_x (L/2^N)$	$R_y (B/2^N)$	$R_{xy}$
$N = 0$	25	15	29.155
$N = 1$	12.5	7.5	14.577
$N = 2$	6.25	3.75	7.289
$N = 3$	3.125	1.875	3.644
$N = 4$	1.563	0.938	1.823
$N = 5$	0.781	0.469	0.911
$N = 6$	0.391	0.234	0.456

Table 2 lists the ablation experiment error for weakly-supervised ViF-SD2Ec in Experiment A. The exploration (Un-EM) is indispensable to explore the hidden paradigm of the neural signal. Therefore, Un-EM and Un-EM&LSTM are unsupervised methods; Un-EM&SD and ViF-SD2Ec are weakly-supervised methods. From the results of the ablation experiment, the decoding error of ViF-SD2Ec (Global) is about 48.3% lower than that of the unsupervised Un-EM algorithm, is about 24.3% lower than that of the unsupervised Un-EM&LSTM, is about 19.7% lower than that of the weakly-supervised Un-EM&SD (Local), and is about 20.3% lower than that of the weakly-supervised Un-EM&SD (Global). This implies that robust ViF-SD2Ec has certain advantages in neural decoding.

#### 4.4 Corrected values and robustness in ViF-SD2E

Table 3 gives the uncorrected and corrected errors in the training and testing errors in the test. The  $N = 3$  is set, which indicates that the exploration’s outputs have been corrected three times in the movement space/subspace. It can be seen from Table 4 that when  $N = 3$ , the maximum tolerance of the  $xy$ -plane is about 3.644. From Table 3, that after being corrected, the errors are concentrated at about 1.5. In the (A+B)/2, the corrected error is reduced to about 1/6 to 1/7 compared with the uncorrected error, and the test error is about half of the uncorrected error and about three times the correction. This shows that although the correction has a slight error compared with the actual labels, the trained exploitation’s generalization is not affected.

In Figure 8,  $R$  is the robust value, which is also called maximum fault tolerance. The robust values are  $R_x = L/2^N$  on the  $x$ -axis,  $R_y = B/2^N$  on the  $y$ -axis and  $R_{xy} = (R_x^2 + R_y^2)^{1/2}$  (Euclidean distance) on the  $xy$ -plane, as shown in Figure 8. The maximum fault tolerance indicates the robustness between the given noisy values and real target labels. Table 4 shows the maximum robust values of the ViF-SD2E from  $N = 0$  to  $N = 6$ . When  $N = 0$ , the robust value is the largest, where the original movement space is used and the learning is completely unsupervised. When  $N > 0$ , the finger movement uses the weak signals 0/1, and the fault tolerance is gradually reduced because the space/subspace is divided to be smaller. Since  $R$  decreases exponentially as  $N \rightarrow +\infty$ , the robust value  $R$  tends to 0, where the learning is completely supervised.

#### 4.5 Complexity (running time) and convergence of ViF-SD2E

The complexity of ViF-SD2E depends on that of the exploration and exploitation and the ViF/SD module. Of these, the ViF/SD module contains the accumulation of the multiple exploration (or an independent algorithm) and the number of divisions of the space into subspaces. Therefore, it is important to reduce the complexity of the algorithms used. In addition, it also seems to be a P/NP problem in terms of exponentially increasing space size and running time. However, the most ideal state is that the purpose of the ViF/SDE (ViF/SD Exploration) is to obtain the best/optimal values (or

something close to the actual labels) when  $N$  is the smallest. In this paper, we assume that the exploration’s iterations are  $n_1$ , and each iteration time is  $t_1$ ; the exploration’s iterations are  $n_2$ , and each iteration time is  $t_2$ ; ViF/SD is divided into  $n_3$  subspaces, and each run time is  $t_3$ . Then, the consumption of ViF-SD2Ec is about  $(t_1 + t_2n_2 + t_3n_3)n_1$ ; the consumption of ViF-SD2Eo is about  $t_1n_1 + t_2n_2 + t_3n_3$ . Therefore, ViF-SD2Ec consumes much more time than ViF-SD2Eo, which is about  $t_2n_1(n_2 - 1) + t_3n_1(n_3 - 1)$ .

In this paper, in ViF-SD2E, the exploration and exploitation are two independent algorithms, and the value of  $N$  is initially set. We can ensure that ViF-SD2E is convergent as  $N$  increases, see Figure 7. In order to maximize the performance of the model one could develop a new algorithm that includes these ideas; for example, making  $N$  adaptive. In our opinion, this can be a larger workload due to the immaturity of the technology, as it seems to involve carrying out Bayesian inference using Exploitation (the prior turns into a posterior, which turns into a prior again), see Figure 1. Moreover, extrapolating from the current results, the Bayesian pattern of the model is highly likely to be correct.

## 5 Conclusion

In this paper, we proposed a robust weakly-supervised method, called ViF-SD2E, for neural decoding. An encoded sequence of 0/1 signals replaces the actual labels in the movement space/subspace and are used as feedback/interaction between external ViF and SD2E. The potential significances of this paper are: 1) we designed a universal ViF/SD module to enhance the application of the spatial symmetry between the movement predictions and the actual labels; 2) an exploration is employed to explore the original neural signals in the movement space/subspace, and an exploitation is used to make effective use of the corrected values from the SDE (SD Exploration) for future calls to evaluate  $N$ -confidence and is used for prediction, which is referred to as exploration–exploitation (2E); 3) we adopt an unsupervised EM and a supervised LSTM with time-series to decode the movement.

We conducted extensive experiments to verify the effectiveness of our method. The results mainly lead us to conclude that: 1) both the spatial and temporal information from the outside world (ViF) used by the neural activity (SD2E) are essential for neural decoding; 2) by incorporating the ViF/SD module and the 2E training strategy, the proposed method can be close to or even outperform a supervised counterpart. Beside, the degree of supervision can be flexibly controlled via a parameter  $N$ . When  $N = 0$ , the model degenerates into an unsupervised mode, but is equivalent to a supervised model when  $N \rightarrow +\infty$ . So, choosing an appropriate  $N$  can enable the model to fully use the 0/1 signals robustly for noisy target values or movements with recorded partial changes in the measurement setups. Finally, if SD2E together with only neural signals involved in the calculation is regarded as a human brain, we believe that the ultimate goal of ViF-SD2E is to obtain the optimal/satisfactory prediction (or something close to the actual label) when  $N$  is the smallest; just like a baby’s learning process or our learning process when faced with new things.

## 6 Broader impacts in weak-labels and regression

When are the weak labels needed? Bengio et al. published “Deep learning for AI,” stating that external symbols used for communication are converted into internal vectors of neural activity in the brain-like paradigm, as well as having a relationship between system 1 and system 2, and system 1 to guide system 2 [30]. The operation of system 1 is unconscious, rapid, and completely in a state of autonomous control; the operation of system 2 is often associated with subjective experiences of behavior, choice, and concentration [31]. In this framework, we think that SDE (SD Exploration) can be regarded as system 1 and Exploitation as system 2, under given perceptual evidence (ViF). Here, the encoded 0/1 signals can help us focus on which area is the prediction/label in a fixed space or subspace, and the  $N$ -value has the effect of adjusting the self-attention (the resolution of the location) via 0/1 signals.

Can regression and classification be linked? All the regression labels are converted to sequences of 0/1 signals and then fed into the SD module. If the exploration has a strong mining ability,  $N$  is small, and if not,  $N$  is large. Beside, we think it may also have a crucial relationship with neural coding or the distribution of the data, that is, how data with similar characteristics to neural signals is generated. Here, if the symmetry between the decoded unsupervised values and the actual labels is not perfect, the  $N$ -value can be increased to reduce errors/robustness. Last but not least, the exploration’s output will also be converted into 0/1 signals to interact or compare with the given 0/1 signals, and 0/1 is a classification idea. So ViF-SD2E may also be used for both regression or classification/clustering.

## References

- [1] P. Wallisch, M.E. Lusignan, M.D. Benayoun, T.I. Baker, A.S. Dickey, and N.G. Hatsopoulos. *MATLAB for neuroscientists: an introduction to scientific computing in MATLAB*. Academic Press, 2014.

- [2] J.A. Livezey and J.I. Glaser. Deep learning approaches for neural decoding: from cnns to lstms and spikes to fmri. *Briefings in Bioinformatics*, 22(2):1577–1591, 2021.
- [3] J.J. Fan, F. Tian, Y. Du, Z.J. Liu, and G.Z. DAI. Thoughts on human-computer interaction in the age of artificial intelligence. *Scientia Sinica Informationis*, 48(4):361–375, 2018.
- [4] D.J. McFarland and J.R. Wolpaw. Brain-computer interface operation of robotic and prosthetic devices. *Computer*, 41(10):52–56, 2008.
- [5] K.T. Kim, H.I. Suk, and S.W. Lee. Commanding a brain-controlled wheelchair using steady-state somatosensory evoked potentials. *IEEE Transactions on Neural Systems and Rehabilitation Engineering*, 26(3):654–665, 2016.
- [6] M. Hamed, S.H. Salleh, and A.M. Noor. (2016) electroencephalographic motor imagery brain connectivity analysis for bci: a review. *Neural computation*, 28(3):999–1041, 2016.
- [7] A.P. Georgopoulos, J.T. Lurito, M. Petrides, A.B. Schwartz, and J.T. Massey. Mental rotation of the neuronal population vector. *Science*, 243(4888):234–236, 1989.
- [8] M.L. Xue, H.F. Wu, and Y. Zeng. Unsupervised ckf decoding for macaque motor cortical spikes. *Acta Automatica Sinica*, 43:302–312, 2017.
- [9] P.N. Paranjape, M.M. Dhabu, P.S. Deshpande, and A.M. Kekre. Cross-correlation aided ensemble of classifiers for bci oriented eeg study. *IEEE Access*, 7:11985–11996, 2019.
- [10] M.S. Ali, N. Gunasekaran, and M.E. Rani. Robust stability of hopfield delayed neural networks via an augmented lk functional. *Neurocomputing*, 234:198–204, 2017.
- [11] H.F. Wu, J.Y. Feng, and Y. Zeng. Neural decoding for macaque’s finger position: Convolutional space model. *IEEE Transactions on Neural Systems and Rehabilitation Engineering*, 27(3):543–551, 2019.
- [12] Z.Q. Xie, O. Schwartz, and A. Prasad. Decoding of finger trajectory from ecog using deep learning. *Journal of neural engineering*, 15(3):036009, 2018.
- [13] N. Ahmadi, T.G. Constandinou, and C.S. Bouganis. Decoding hand kinematics from local field potentials using long short-term memory (lstm) network. In *In 2019 9th International IEEE/EMBS Conference on Neural Engineering (NER)*, pages 415–419. IEEE, 2019.
- [14] W. Bishop. Semi-supervised classification for intracortical brain-computer interfaces. ml.cmu.edu, 2013.
- [15] J.Y. Feng, H.F. Wu, Y. Zeng, and Y.H. Wang. Weakly supervised learning in neural encoding for the position of the moving finger of a macaque. *Cognitive Computation*, 12(5):1083–1096, 2020.
- [16] D. Zhang, J. Han, L. Zhao, and T. Zhao. From discriminant to complete: Reinforcement searching-agent learning for weakly supervised object detection. *IEEE Transactions on Neural Networks and Learning Systems*, 31(12):5549–5560, 2020.
- [17] E. Xie, J. Ding, W. Wang, X. Zhan, and P. Luo. Detco: Unsupervised contrastive learning for object detection. In *arXiv*. arXiv:2102.04803v2, 2021.
- [18] T. Chen, S. Saxena, L. Li, D.J. Fleet, and G. Hinton. Pix2seq: A language modeling framework for object detection. *arXiv*, 2021.
- [19] V. Gilja, P. Nuyujukian, C.A. Chestek, J.P. Cunningham, B.M. Yu, J.M. Fan, M.M. Churchland, M.T. Kaufman, J.C. Kao, S.I. Ryu, and K.V. Shenoy. A high-performance neural prosthesis enabled by control algorithm design. *Nature Neuroscience*, 15(12):1252–1257, 2012.
- [20] G. Czanner, U.T. Eden, S. Wirth, M. Yanike, W.A. Suzuki, and E.N. Brown. Analysis of between-trial and within-trial neural spiking dynamics. *Journal of neurophysiology*, 99(5):2672–2693, 2008.
- [21] M.M. Shanechi, G.W. Wornell, Z.M. Williams, and E.N. Brown. Feedback-controlled parallel point process filter for estimation of goal-directed movements from neural signals. *IEEE Trans. Neural Syst. Rehabil. Eng.*, 21(1):129–140, 2013.
- [22] P.H. Tseng, N.A. Urpi, M. Lebedev, and M. Nicolelis. Decoding movements from cortical ensemble activity using a long short-term memory recurrent network. *Neural computation*, 31(6):1085–1113, 2019.
- [23] V. Elango, A.N. Patel, K.J. Miller, and V. Gilja. Sequence transfer learning for neural decoding. In *bioRxiv*, page 210732. doi: <https://doi.org/10.1101/210732>, 2017.
- [24] G. Pan, J.J. Li, Y. Qi, H. Yu, J.M. Zhu, X.X. Zheng, Y.M. Wang, and S.M. Zhang. Rapid decoding of hand gestures in electrocorticography using recurrent neural networks. *Frontiers in neuroscience*, 12:555, 2018.
- [25] J.Y. Feng, H.F. WU, and Y. Zeng. Neural decoding for location of macaque’s moving finger using generative adversarial networks. In *IEEE International Conference of Intelligent Robotic and Control Engineering*, pages 213–217. IEEE, 2018.
- [26] D. Sussillo, S.D. Stavisky, J.C. Kao, S.I. Ryu, and K.V. Shenoy. Making brain–machine interfaces robust to future neural variability. *Nature communications*, 7:13749, 2016.
- [27] A.C. Smith, L.M. Frank, S. Wirth, M. Yanike, D. Hu, Y. Kubota, A.M. Graybiel, W.A. Suzuki, and E.N. Brown. Erratum: Dynamic analysis of learning in behavioral experiments. *Journal of Neuroscience*, 25(12):447–461, 2005.
- [28] T.Q. Chen and C. Guestrin. Xgboost: A scalable tree boosting system. In *Proceedings of the 22nd acm sigkdd international conference on knowledge discovery and data mining*, pages 785–794. ACM, 2016.

- [29] G.L. Ke, Q. Meng, T. Finley, T.F. Wang, W. Chen, W.D. Ma, Q.W. Ye, and T.Y. Liu. Lightgbm: A highly efficient gradient boosting decision tree. In *Advances in Neural Information Processing Systems*, pages 3146–3154. NeurIPS, 2017.
- [30] Y. Bengio, Y. Lecun, and G. Hinton. Deep learning for AI. *Communications of the ACM*, 64(7):58–65, 2021.
- [31] K. Daniel. *Thinking, Fast and Slow*. Farrar, Straus and Giroux, 2012.

## A Parameter and running environment

The operating environment of KF, XGBoost, LightGBM, WSL-KF, and WSL-EM is as follows. The PC operation system running the decoding algorithms is Windows 10 professional 64-bit DirectX 12, the processor is Intel Corei7-9700@3.00GHz eight-core, and the processing software is MatLabR2020b\_Win. Also, the operating environment of the LSTM and ViF-SD2E is as follows. The 4U rack server operating system running the decoding algorithms is UBUNTU 20.04.1, the barebone system is SYS-4029GP-TRT, the processor is Intel Xeon Gold 6226R 2.90G/16Core/22M/150W, the GPU computing card is NVIDIA RTX 3090 24G memory, and the processing software is python 3.8.8 and MatLab R2020b\_Linux. Moreover, the parameters were set as follows.

**KF:** The initial position  $z_0 = 0$ , covariance  $P_{y,0|0} = 10$ , state noise variance  $Q_w = 0.8$ , and observed noise variance  $\mathbf{R}_v = (\bar{\mathbf{s}} - \hat{\mathbf{s}})^T(\bar{\mathbf{s}} - \hat{\mathbf{s}})/(K - 1)$ , where  $\bar{\mathbf{s}} = (\mathbf{s}_0, \mathbf{s}_1, \dots, \mathbf{s}_{K-1})^T$  and  $\hat{\mathbf{s}} = \mathbf{Y}^\dagger \tilde{\mathbf{W}}$ . **XGBoost:** The initial  $max\_depth = 5$ ,  $learning\_rate = 0.1$ ,  $n\_estimators = 150$ ,  $objective = 'reg : linear'$ ,  $n\_jobs = -1$ ,  $eval\_metric = 'logloss'$ , and  $verbose = 100$ . **LightGBM:** The initial  $num\_leaves = 33$ ,  $learning\_rate = 0.05$ ,  $n\_estimators = 150$ ,  $eval\_metric = 'logloss'$ , and  $verbose = 100$ . **WSL-KF:** This is the KF in WSL. The initial position  $z_0 = 10$ , covariance  $P_{y,0|0} = 10$ , and system noise variance  $R_w = 0.8$ . The observed noise variance  $\mathbf{R}_v = \text{diag}(\text{ones}(1,42))$  represents generation behavior 1, and the diagonal matrix is listed as 42. The initial weight  $\tilde{\mathbf{W}}_0 = \text{ones}(2, 42)$  represents generation behavior 2, and the all-ones matrix is listed as 42. **WSL-EM:** This is the EM in WSL. The initial position  $z_0 = 10$ , covariance  $P_{y,0|0} = 10$ , and system noise variance  $R_w = 2$ . The observed noise variance  $\mathbf{R}_v = \text{diag}(\text{ones}(1, 42T))$  represents generation behavior 1 and the diagonal matrix is listed as  $42T$ .  $\tilde{\mathbf{W}}_0 = \text{ones}(2, 42T)$  represents generation behavior 2, the all-ones matrix is listed as  $42T$ . The  $T$  is set to 10 in the X- and Y-position, and  $iteration = 8$ . **LSTM:** The initial,  $input\_size = 42T$ ,  $hidden\_size = 70$ ,  $output\_size = 1$ ,  $num\_layers = 3$ ,  $learning\_rate = 0.02$ . The maximum-value of  $epoch$  is set to 1000, and optimization period  $t = 10$ . The Look\_back  $T$  is also set to 10 in the X- and Y-position. **ViF-SD2E (Local) and (Global):** Both of these are robust weakly-supervised methods. The initial position  $z_0 = 10$ , covariance  $P_{y,0|0} = 10$ , and system noise variance  $R_w = 2$ . The observed noise variance  $\mathbf{R}_v = \text{diag}(\text{ones}(1, 42T))$  represents generation behavior 1 and the diagonal matrix is listed as  $42T$ .  $\tilde{\mathbf{W}}_0 = \text{ones}(2, 42T)$  represents generation behavior 2, the all-ones matrix is listed as  $42T$ . The  $input\_size = 42T$ ,  $hidden\_size = 70$ ,  $output\_size = 1$ ,  $num\_layers = 3$ ,  $learning\_rate = 0.02$ . The maximum value of  $epoch$  is set to 1000. The Look\_back  $T$  is also set to 10 in the X- and Y-position, and the value of  $iteration$  is set to 8. Finally, the space parameter  $N$  is set to 3 in the X- and Y-position.

For non-deep methods, the experiments of KF, XGBoost, LightGBM, WSL-KF, and WSL-EM can be directly reproduced. For deep LSTM and ViF-SD2E, the underlying LSTM adopted in the exploitation has the same settings as traditional supervised LSTM for the sake of making a fair comparison in the testing.